High-performance, low-cost on-chip Fabry-Perot interferometer with microfluidic channel using single anisotropic wet etching

Régis Guertin, Thomas Lacasse, Cédric Lemieux-Leduc, Marc-Antoine Bianki, Yves-Alain Peter

***Abstract*—In this paper, we present a design for improving the fabrication process of an in-plane Fabry-Perot interferometer (FPI). The fabrication process involves a single anisotropic etching step in silicon (110) to form a resonator featuring a microfluidic channel and perpendicular structures for fiber alignment. The process etches along the crystalline planes, resulting in an almost perfectly parallel resonant cavity and reducing roughness of optical components. The FPI mirrors consist of two (111) planes coated with a thin film of evaporated gold, enhancing reflectivity. The advantage of this process is that it enables low-cost and commercial fabrication while maintaining high performance. Resonances with Q factor exceeding 2×10^3 are reported.**

***Index Terms*—Fabry-Perot, Silicon (110), Micromirrors, Anisotropic Etching, Vertical etching, Microfluidics.**

I. Introduction

Extensive research has been conducted on studying the parameters of the fabrication process to enhance the performance of on-chip Fabry-Perot Interferometers (FPIs). The reflectivity, parallelism, and surface roughness of the mirrors are factors that determine the FPI's finesse and Q factor, both of which rely therefore on the fabrication quality [1]. A larger finesse leads to improved accuracy in measuring wavelength resonances within the cavity, which enhances the performance of wavelength displacement sensors. On-chip FPIs find use in various applications such as gas sensing [2], [3], tunable optical filters [4], [5], refractive index measurements [6], [7], and refractive index cytometry [8], [9]. Micromachining techniques have allowed the fabrication of precise and reliable micrometer-sized in-plane resonators. In-plane orientation is preferred for FPIs, as it facilitates encapsulation with optical fibers. To fabricate such resonators, deep reactive ion etching (DRIE) is widely employed [6], [10]. However, this technique has issues with verticality deviation and scalloping, which affects optical performances. The former leads to a ±0.5° deviation in parallelism and is a major issue [1]. The latter causes surface roughness on mirrors ranging from 30nm to 200nm based on etching parameters. To overcome the roughness caused by scalloping, some groups used DRIE etching, followed by anisotropic wet smoothing [4], [11], [12] or cryogenic process [13]. Although roughness is reduced, these techniques require additional steps to align the device along the <112> crystalline direction or specialized equipment. Other techniques, such as sidewall smoothing with focused ion beam, were studied but are not realistic for large-scale production [14].

In this paper, we propose a simple and cost-effective fabrication method and design to optimize the parallelism of the mirrors while reducing roughness, as compared to DRIE etching methods. The design also includes a microfluidic channel for measuring the refractive index or swelling of different liquids and polymers, along with optical fiber grooves for packaging purposes. By using liquid anisotropic TMAH etching and a silicon (110) substrate, we demonstrate that it is possible to manufacture the various structures in a single etching step.

II. Fabrication

A. Design on Silicon (110)

Figure 1 depicts a complete device composed of a vertically etched FPI, which achieves a high degree of parallelism by utilizing the crystalline properties and orientation of silicon (110). The (110) planes are etched to reveal the vertical (111) planes, whose etching rate is orders of magnitude lower than that of both the (100) and (110) planes. As a result, intriguing

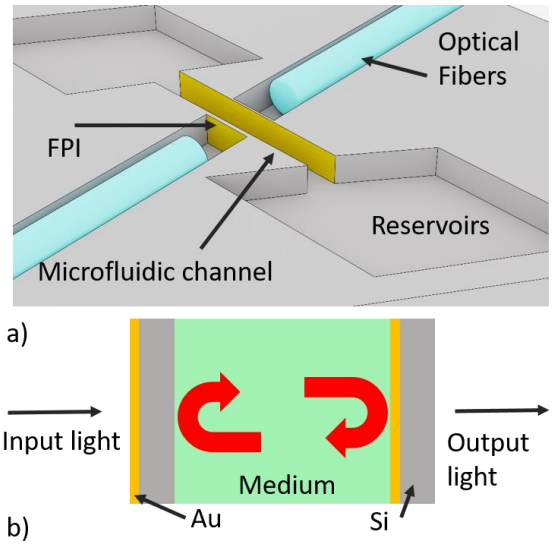

Fig. 1. a) FPI with microfluidic channel, fiber grooves and reservoirs for liquid. b) Side view of the FPI. Silicon is shown in gray, gold in yellow and medium under test in green.

shapes can be etched. For instance, when etching a circular pattern, a hexagonal shape with two slanted walls and two pairs of vertical walls are revealed. For this method, we are only interested in the pair of (111) planes along the <112> direction, which enables easy fabrication of in-plane FPI. However, the downside of this method is the under-etching of convex corners causing all convex structures to be etched in unintended but predictable directions, thus limiting the design of complex structures. Compensation structures in the shape of rectangular beams can be used to overcome this issue [15]. The mask pattern design proposed in Fig. 2 can accommodate compensation structures of different lengths seamlessly. The patterns are oriented along either the <110> or <112> direction families. The length of the beams is determined by the etch depth and the etchant used. By using this design, all compensation structures can be oriented in the same direction, which simplifies the determination of their geometry. However, the corresponding length needs to be measured experimentally from test structures prior to designing the device, as etch rates vary depending on the temperature, solution, and orientation of the sample in the solution. For the presented design, the beam length and width were established to be 110µm and 10µm respectively. Since perpendicular structures cannot be etched in (110) silicon, it is challenging to design fiber grooves that are perpendicular to the resonator. In Fig. 2c, a design is shown that allows for a vertical groove in the <11¯1> direction that is perpendicular to the resonator. This design consist of an array of intertwined blended parallelograms with compensation beams. The width of the groove is 250µm, and the compensation beams have a length of 110µm and are spaced by 80µm. Since the sides of the grooves are not in the <112> or <110> directions, the sidewalls of these grooves will have high roughness. The tolerance on the roughness and verticality of the sidewalls is very high since they are not optical components. However, the optical quality of the (111) etched stop plane in the <112> direction remains high.

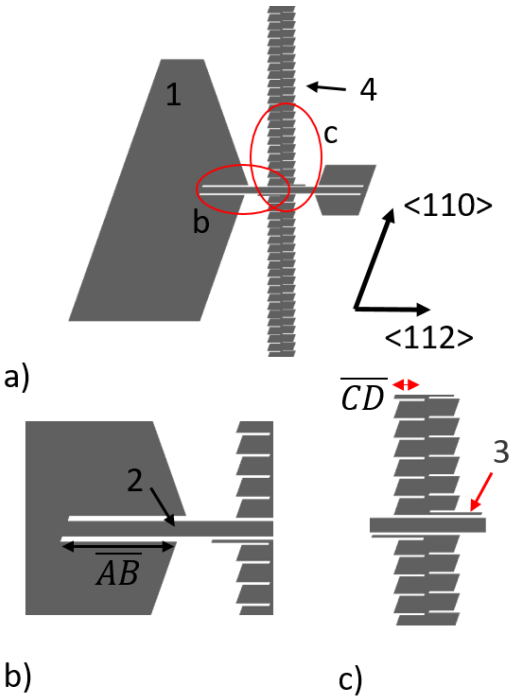

Fig. 2. a) Mask design of the devices. b) Interface of the reservoirs and the micro fluidic channel c) Fiber grooves with compensation structures. 1- Liquid reservoirs. 2- Microfluidic channel. 3- Vertical mirrors. 4- Fiber grooves.

B. Process flow

The fabrication process begins with a p-doped (10Ωm) silicon wafer with a (110) crystaline orientation. The wafer is thermally oxidized at 950°C to produce an oxide layer with a thickness of 300nm. To reveal the crystal planes, an alignment fork pattern [16] is etched in the oxide layer using buffered hydrofluoric acid solution (BHF) and dipped in TMAH 25% for 10min. The fork pattern enables a 0.05° alignment precision with the <112> directions. The device pattern is then transferred to the oxide using BHF and subsequently etched into silicon using TMAH 25% for 75min to achieve a depth of 90µm, which enables the positioning of the optical fiber at the bottom of the grooves. Finally, 60nm of gold is evaporated at a 35° angle to increase the reflectivity while coating only one side of each mirror of the resonator. Non-conformal deposition prevents the formation of undesired parasitic cavities. A micrograph of the fabricated device is shown in Fig. 3. The perpendicular structure is well defined with two thin silicon mirrors and with two long

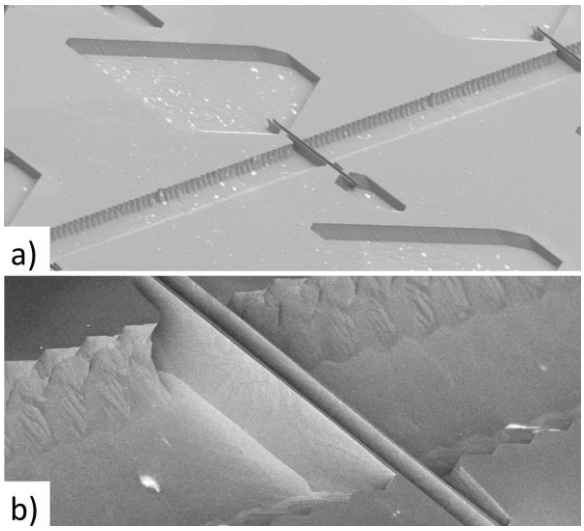

Fig. 3. SEM images of the fabricated device. a) Overview of the whole device. b) Close up view on the resonator.

straight grooves. The microfluidic channel is connected to both reservoirs. Using white light interferometry, the surface roughness on the (111) vertical plane was measured to be as low as 40nm, which is notably less than what is obtained with DRIE techniques alone. In order to measure the roughness, a sample was cleaved in a direction parallel to that of the mirrors and rotated to expose the (111) plane. Using white light interferometry (Fogale Photomap 3D Optical Profiler), the surface roughness was measured to be as low as 40nm, which is notably less than what is obtained with DRIE techniques.

The side walls of the fiber grooves exhibit low-frequency roughness, as anticipated, with a frequency comparable to that of the compensation pattern removed during etching. The compensation patterns in the reservoirs were designed to be longer than necessary and, consequently, are not entirely etched away. In order to measure the parallelism of the mirrors,

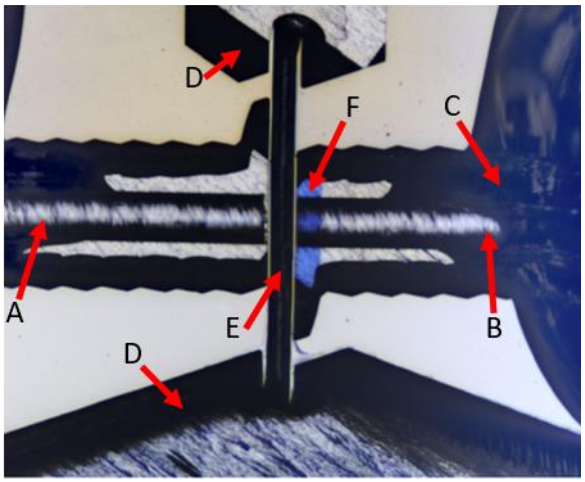

Fig. 4. Assembled device. Blue section (F) is a shadow caused by the mirrors. A and B- Input and output fiber. C- Optical glue to bond fibers to the sensor. D- Reservoirs. E- Microfluidic channel and Fabry-Perot interferometer.

the sample was cut perpendicularly to the microfluidic channel using a dicing saw. SEM was used to determine an angle of 0.03° between the mirrors, as illustrated in Fig. 5.

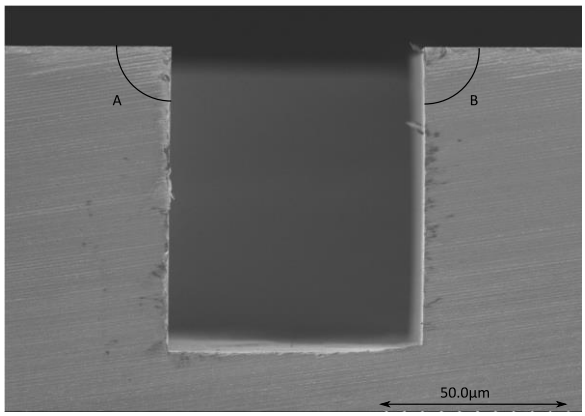

Fig. 5. Cross-section of the microfluidic channel showing the verticality of the structure. Angle *A* was measured at 89.92° and *B* at 90.11°

III. Optical Characterisation of the Assembled Device

Figure 4 shows the assembled device. A tunable laser (Keysight-N7776C) synchronized with photodiodes (Keysight-N7745C) was used to measure the transmission spectrum of the device, as depicted in Fig. 6. Light coupling was achieved by placing two SMF-28 optical fibers at a distance of approximately 5µm to 20µm from the outwardside of both mirrors. The measured Q factor, finesseand full width at half-maximim (FWHM) are respectively

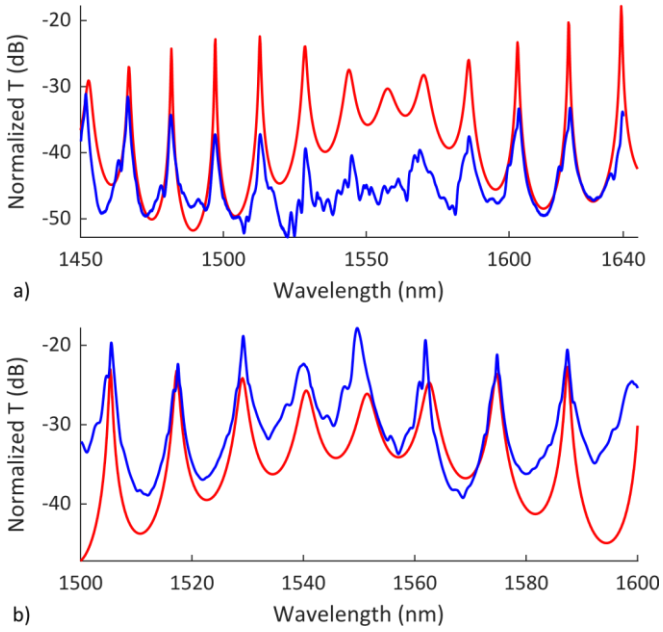

Fig. 6. Experimental (blue) and calculated (red) transmission spectrum from FPI. a) Empty cavity with width of silicon, gold and microfluidic channel being respectively 2.59µm, 60nm and 68.9µm b) Cavity filled with PDMS with width of silicon, gold and microfluidic channel being respectively 2.56µm, 60nm and 68.0µm

1.3×10^3, 13.5 and 1.10nm for the first cavity (Fig. 6a) and 2.2×10^3, 17.1 and 0.66nm for the second (Fig. 6b). The transfer matrix method was used to calculate the FPIs transmissions [1], and the results are illustrated in Fig. 6. The FPIs transmissions were calculated using the transfer matrix method presented by St-Gelais [1], with the results being illustrated in Fig. 6. The method involves utilizing the transfer matrix of each interfaces, while accounting for the divergence of the Gaussian beam and roughness. In this case, the measured roughness of 40nm was incorporated in the simulation. The experimental responses shows a good agreement with the simulated spectra in terms of peak positions and amplitudes. According to FPI theory, the simulated spectra are expected to have constant peak powers, but the simulation model includes a dual Fabry-Perot cavity, consisting of one formed by the two highly reflective gold layers, and the other formed by a gold layer and the silicon layer with the air interface, which creates a parasitic cavity. The parasitic cavity is formed by a FPI with a different FSR than the main cavity and is dependent on the resonance order in the silicon structure determined through Equation 1,

$$L = \frac{m\lambda}{2n}. \tag{1}$$

Here, m represents the resonance order, λ =1550nm is the central wavelength, and the refractive index of silicon is n_{Si} = 3.48. The effect of this parasitic cavity is observed when the peaks broaden, as can be seen experimentally in Fig. 6a from 1540nm to 1580nm and in Fig. 6b from 1540nm to 1560nm, depending on fabrication variations and optical path length. Simulations of this effect for different values of silicon widths, represented by the parameter *m*, are shown

in Fig. 7. m takes integer values in Fig. 7a and $m + \frac{1}{2}$ in Fig. 7b. For integer and small values of m, the parasitic cavity in the central wavelength generates no attenuation. However, for $m + \frac{1}{2}$, attenuation is present in the central wavelength causing low amplitude and broadened peaks. This parasitic cavity causes destructive interference and reduces the overall finesse of the cavity. The cavities fabricated for this experiment have a resonance order of approximately m = 11.5 at a central wavelength of 1550nm, thus exhibiting destructive interference in the silicon layer. However, the interference is constructive for wavelength of 1500nm, hence higher finesse in this region. Ideally, the silicon structure would have a width of 223nm for a resonance of m = 1, but this is difficult to achieve without proper lithography tooling. Surface roughness and non-parallelism of the mirrors are factors that decreases the finesse as well. Improvements to the wet etching method could increase performance by reducing roughness and increasing the parallelism. Figure 6a shows that the parasitic

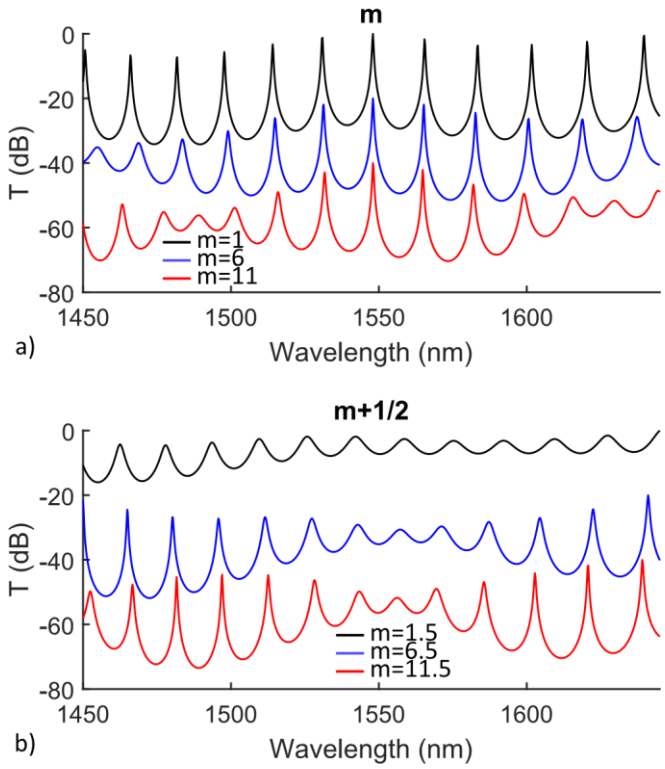

Fig. 7. Simulated transmission spectrum in arbitrary units as a function of the order of resonance and the size of the silicon mirror width. a) Resonance order takes the value of an integer, denoted as m b) Resonance order takes values of m +1/2, where m is an integer.

cavity lowers the finesse of the device, resulting in low peak amplitude from 1540nm to 1580nm. To reduce the resonance order, the thickness of the silicon wall must not exceed 223nm. This is determined using Equation 1,

$$L = \frac{m\lambda}{2n} \tag{2}$$

where m = 1 represents the resonance order, λ =1550nm is the central wavelength, and the refractive index of silicon is n_{Si} = 3.48. Using the Fresnel equation (Equation 3), the parasitic reflectivity is estimated to be around 30%, with n_{Air} = 1.

$$r = \left| \frac{n_{Si} - n_{Air}}{n_{Si} + n_{Air}} \right|^2 \tag{3}$$

Design-wise, it is possible to reduce the impact of the parasitic cavity on the transmission spectrum by changing the process flow to have the gold layers facing each other, but this would increase the fabrication complexity. Alternatively, thinned silicon structures can achieve similar results while maintaining the presented design.

IV. Conclusion

In this study, we developed a low-cost fabrication method for an in-plane FPI that includes fiber grooves, a microfluidic channel, and reservoirs. Our technique used TMAH etching and compensation structures to achieve perpendicular features with silicon (110). The technique is easy to implement and requires less expensive tooling for higher performances. We measured the device's quality factor to be 2.2×10^3, indicating high performance. In the future, we plan to explore the potential of these FPIs for gas detection applications.

Acknowledgments

We would like to thank CMC for supporting the fabrication and Coventor MP for the acces to SEMulator 3D software.

V. References Section

References

[1] R. St-Gelais, A. Poulin, and Y.-A. Peter, "Advances in modeling, design, and fabrication of deep-etched multilayer resonators," *Journal of Lightwave Technology*, vol. 30, no. 12, pp. 1900–1908, jun 2012.

[2] R. St-Gelais, G. Mackey, J. Saunders, J. Zhou, A. Leblanc-Hotte, A. Poulin, J. A. Barnes, H.-P. Loock, R. S. Brown, and Y.-A. Peter, "Gas sensing using polymer-functionalized deformable Fabry-Perot interferometers," *Sensors and Actuators B: Chemical*, vol. 182, pp. 45–52, 2013.

[3] R. Guertin, M.-A. Bianki, C. Lemieux-Leduc, and Y.-A. Peter, "Multigas detection using Fabry-Perot interferometers on silicon chip," *Sensors and Actuators B: Chemical*, p. 129655, 2021.

[4] A. Lipson and E. M. Yeatman, "A 1-D photonic band gap tunable optical filter in (110) silicon," *Journal of Microelectromechanical Systems*, vol. 16, no. 3, pp. 521–527, 2007.

[5] J. Masson, R. St-Gelais, A. Poulin, and Y.-A. Peter, "Tunable fiber laser using a MEMS-based in plane Fabry-Perot filter," *IEEE Journal of Quantum Electronics*, vol. 46, no. 9, pp. 1313–1319, 2010.

[6] R. St-Gelais, J. Masson, and Y.-A. Peter, "All-silicon integrated FabryPerot cavity for volume refractive index measurement in microfluidic´ systems," *Applied physics letters*, vol. 94, no. 24, p. 243905, 2009.

[7] N. Gaber, Y. M. Sabry, M. Erfan, F. Marty, and T. Bourouina, "High-Q Fabry–Perot micro-cavities for high-sensitivity volume refractometry," *Micromachines*, vol. 9, no. 2, p. 54, 2018.

[8] A. Leblanc-Hotte, G. Chabot-Roy, L. Odagiu, M. Richaud, S. Lesage, J.-S. Delisle, and Y.-A. Peter, "High-throughput refractive index-based microphotonic sensor for enhanced cellular discrimination," *Sensors and Actuators B: Chemical*, vol. 266, pp. 255–262, 2018.

[9] A. Leblanc-Hotte, N. S. Nkwe, G. Chabot-Roy, E. B. Affar, S. Lesage, J.-S. Delisle, and Y.-A. Peter, "On-chip refractive index cytometry for whole-cell deformability discrimination," *Lab on a Chip*, vol. 19, no. 3, pp. 464–474, 2019.

[10] N. Gaber, A. Altayyeb, S. A. Soliman, Y. M. Sabry, F. Marty, and T. Bourouina, "On-channel integrated optofluidic pressure sensor with optically boosted sensitivity," *Sensors*, vol. 19, no. 4, p. 944, 2019.

[11] D. Lee, K. Yu, U. Krishnamoorthy, and O. Solgaard, "Vertical mirror fabrication combining KOH etch and DRIE of (110) silicon," *Journal of Microelectromechanical Systems*, vol. 18, no. 1, pp. 217–227, 2009.

[12] S.-S. Yun, S.-K. You, and J.-H. Lee, "Fabrication of vertical optical plane using DRIE and KOH crystalline etching of (110) silicon wafer," *Sensors and Actuators A: Physical*, vol. 128, no. 2, pp. 387–394, 2006.

[13] M. W. Pruessner, W. S. Rabinovich, T. H. Stievater, D. Park, and J. W. Baldwin, "Cryogenic etch process development for profile control of high aspect-ratio submicron silicon trenches," *Journal of Vacuum Science & Technology B: Microelectronics and Nanometer Structures Processing, Measurement, and Phenomena*, vol. 25, no. 1, pp. 21–28, 2007.

[14] I.-H. Song, Y.-A. Peter, and M. Meunier, "Smoothing dry-etched microstructure sidewalls using focused ion beam milling for optical applications," *Journal of micromechanics and microengineering*, vol. 17, no. 8, p. 1593, 2007.

[15] P. Pal, M. A. Gosalvez, K. Sato, H. Hida, and Y. Xing, "Anisotropic etching on Si{110}: experiment and simulation for the formation of microstructures with convex corners," *Journal of Micromechanics and Microengineering*, vol. 24, no. 12, p. 125001, oct 2014.

[16] M. Vangbo and Y. Backlund, "Precise mask alignment to the crystallographic orientation of silicon wafers using wet anisotropic etching," *Journal of Micromechanics and Microengineering*, vol. 6, no. 2, pp. 279–284, jun 1996.